Journal of Structural Engineering & Applied Mechanics (2025) 8(4):373-399
DOI 10.31462/jseam.2025.04373399

RESEARCH ARTICLE

Evaluation of the influence of ground acceleration on the seismic performance of typical RC buildings designed according to the 1975 Turkish Earthquake Code

Oguzhan Celebi[1*]

[1] Atatürk University, Department of Civil Engineering, Erzurum, Türkiye

Article History

Received 19 November 2025
Accepted 25 December 2025

Keywords

Kahramanmaraş earthquake
Ground acceleration
Frequency analysis
Time-history analysis
Inter-story drift
Reinforced concrete structures

Abstract

The ground accelerations recorded during the February 6, 2023, Kahramanmaraş earthquakes exceeded the design acceleration values specified by the Turkish Earthquake Codes enforced between 1975 and 2018. This paper examines the effect of ground acceleration intensity on the seismic performance of typical RC buildings that are representative of the construction practice governed by the 1975 Earthquake Code and the TS 500 standard. Within this scope, two hypothetical RC frame buildings with equal story numbers and with similar plan areas, assumed to be located in the Hatay–Defne region, were modeled. Both buildings were designed according to the provisions of the 1975 code; however, one building was configured to have a regular and symmetric plan layout, while the other one had a plan and asymmetric stiffness distribution. Equivalent static analyses based on the 1975 code and linear time-history analyses by using the real ground motion records, including the record of the February 6, 2023, Pazarcık event, spectrally scaled according to TBEC 2018, were performed. The seismic responses of the buildings were evaluated in terms of floor accelerations, top displacements, base shear forces, and inter-story drifts. In addition, the natural periods and frequency contents obtained by FFT analyses are examined. The results indicate that although increasing ground acceleration significantly amplifies seismic demands in both buildings, the presence of plan irregularity and non-uniform stiffness distribution leads to markedly higher drift and acceleration demands. Consequently, it is concluded that ground acceleration alone cannot explain any probable collapses, and structural configuration and code-based design assumptions play a decisive role in the seismic performance of RC buildings that were designed according to the 1975 Earthquake Code.

1. Introduction

Türkiye is situated in a seismically active region formed by the conjunction of the Anatolian Plate with the Eurasian Plate in the north and the Arabian Plate in the south. The North Anatolian Fault Zone (NAFZ) and the East Anatolian Fault Zone (EAFZ) are the most seismically active fault lines in Türkiye. The westward extrusion of the Anatolian Plate makes the periodic occurrence of large earthquakes easier for the release of

* Corresponding author (celebioguzhan@atauni.edu.tr)

eISSN 2630-5763 © 2025 Authors. Publishing services by golden light publishing®.
This is an open-access article under the CC BY-NC-ND license (http://creativecommons.org/licenses/by-nc-nd/4.0/).

accumulated strain in these fault lines. Important earthquakes that took place in Türkiye, such as the Erzincan Earthquake of 1939, the Kocaeli Earthquake of 1999, the Van Earthquake of 2011, and the Elazığ Earthquake of 2020, offered convincing evidence related to the seismic vulnerability of existing buildings in Türkiye [1–5].

The seismic series on February 6, 2023, including Pazarcık (Mw 7.7) and Elbistan (Mw 7.6), is one of the most destructive ones in the seismic history of the Republic. These earthquakes affected a region of about 110,000 km² and caused over 60,000 deaths and drastic damage to hundreds of thousands of buildings [6, 7]. The horizontal PGA and vertical PGA were observed above 2 g and 1 g, respectively, at multiple stations based on strong-motion data analysis, and design spectra defined by the Turkish Building Earthquake Code 2007 (DBYBHY 2007) and Turkish Building Earthquake Regulation 2018 (TBEC 2018) were also violated in multiple instances [2-5]. These results indicate significant amounts of ground motion amplification caused by near-field effects, directivity, and regional characteristics. About 50% of buildings in Türkiye were built before 2000, and most of them were comprised of low-rise RC frame buildings [8-10]. They were designed under the 1975 Earthquake Code, which allowed a suitable design value of 0.1 g for the first-degree zones, but almost no information could be gathered about ductility, regularity, and other design requirements [11]. On the other hand, TBEC 2018 defined the spectral acceleration values depending on the location and used modern design approaches for seismic design. Nevertheless, the recorded accelerations during the 2023 series were over the design limits defined by both DBYBHY 2007 and TBEC 2018, and solely depending on design acceleration values cannot provide seismic safety [3, 6].

Although ground acceleration significantly influences building responses during earthquakes, it is well acknowledged that acceleration amplitude alone cannot comprehensively account for structural damage. Prior research has established that earthquake duration, frequency content, energy parameters, and local soil conditions strongly influence structural behavior, and that records with comparable peak accelerations can result in markedly different damage levels [12–28]. Subsequent field investigations following the earthquakes on February 6, 2023, revealed that substantial damage was primarily associated with low concrete strength, insufficient transverse reinforcement, weak-storey mechanisms, and discontinuities within the load-bearing system, even in regions subjected to analogous ground acceleration levels [29–32]. In this context, the present study investigates the influence of ground acceleration intensity on the seismic performance of two theoretical reinforced concrete building models that represent standard constructions designed in line with the 1975 Turkish Earthquake Code. The two models have the same number of floors, the same size of plan area, and the same material properties. But their structures are set up in distinct ways. The S1 model has an uneven structure with an irregular plan shape and stiffness distribution, while the S2 model has a regular and symmetrical structure. The primary objective of the study is to demonstrate that ground acceleration alone cannot account for structural failure, and that the configuration and rigidity of designs are critical to their performance during earthquakes. To achieve this objective, the design spectral acceleration values delineated in the 1975 and 2018 Turkish Earthquake Codes are compared with the actual ground motion records from the February 6, 2023, Kahramanmaraş earthquakes. Assessments of analogous seismic loads and linear time histories employing spectrally scaled ground motion data are performed for both structure models. We compare the reactions of acceleration, displacement, base shear, and interstory drift. The results show that going above the design spectral accelerations does not always cause a collapse. Instead, the way that reinforced concrete structures built according to the 1975 code respond to earthquakes is mostly affected by how they are built and how stiff they are.

This study exclusively examines linear elastic analysis methods that adhere to the analytical framework established by the 1975 Turkish Earthquake Code. The primary objective of the study is not to predict collapse mechanisms or post-yield behavior, but to do a comparative investigation of the impacts of ground acceleration intensity and structural design, particularly plan regularity and stiffness distribution, on seismic

demand parameters. Consequently, the results are examined using demand-based response measures, such as interstory drift ratios, stress distributions, and acceleration amplification. Nonlinear behavior, plastic hinge formation, and collapse mechanisms are essential for the performance-based assessment of existing structures; nonetheless, they are considered beyond the scope of the current study and are recommended as critical domains for future research development.

2. Material and method

To create a standard way to analyze how a typical reinforced concrete building built according to the 1975 Turkish Earthquake Code would behave in an earthquake, two different hypothetical building models were made. Both models had the same geometric properties but different lateral stiffness distributions. S1 is a structure with an uneven distribution of stiffness and an irregular plan, while S2 is a structure with a regular and symmetric arrangement. It was thought that both of them were in the Hatay–Defne area, where substantial ground vibrations were felt during the Kahramanmaraş earthquakes on February 6, 2023. This part goes into great length into the features of these building models, the design ground acceleration factors set out in the Turkish Earthquake Codes, and the analytical methods used in the study.

2.1. Investigated buildings

Two reinforced concrete buildings were modeled in this study to have the same structural features as buildings built pursuant to the 1975 Turkish Earthquake Code (ABYBHY-1975). Both structures were intended to be in Hatay Province, Türkiye, which shook a lot during the Pazarcık (Mw 7.7) and Elbistan (Mw 7.6) earthquakes on February 6, 2023. Both models have the same number of stories and the same material properties, and their plans are about the same size. However, their lateral stiffness distribution and plan arrangement are different. S1 has an uneven stiffness distribution and an irregular plan, while S2 has a regular and symmetric architecture. Table 1 shows the geometric shapes, material qualities, and cross-sectional sizes that were used for both models.

Table 1. Comparison of structural and material properties of the investigated buildings

Parameter	S1 Model	S2 Model
Number of Stories	Ground + 4 Typical Stories	Ground + 4 Typical Stories
Story Height (m)	3.0	3.0
Total Building Height (m)	15.0	15.0
Structural System	RC frame without shear walls	RC frame without shear walls
Concrete / Reinforcement Class	C14 / S220	C14 / S220
Column Dimensions (cm)	20×60 – 25×65	25×65
Beam Dimensions (cm)	25×50 – 30×60	25×50 – 30×60
Average Column Reinforcement Ratio (%)	1.2–1.4	1.5–1.7
Average Beam Reinforcement Ratio (%)	1.0–1.3	1.2–1.5
Soil Class (per TBEC 2018)	ZC	ZC
Material Strength (MPa)	fck = 14, fyk = 220	fck = 14, fyk = 220
Model Type	Moment-resisting frame	Moment-resisting frame
Slab Type	Monolithic RC slab	Monolithic RC slab

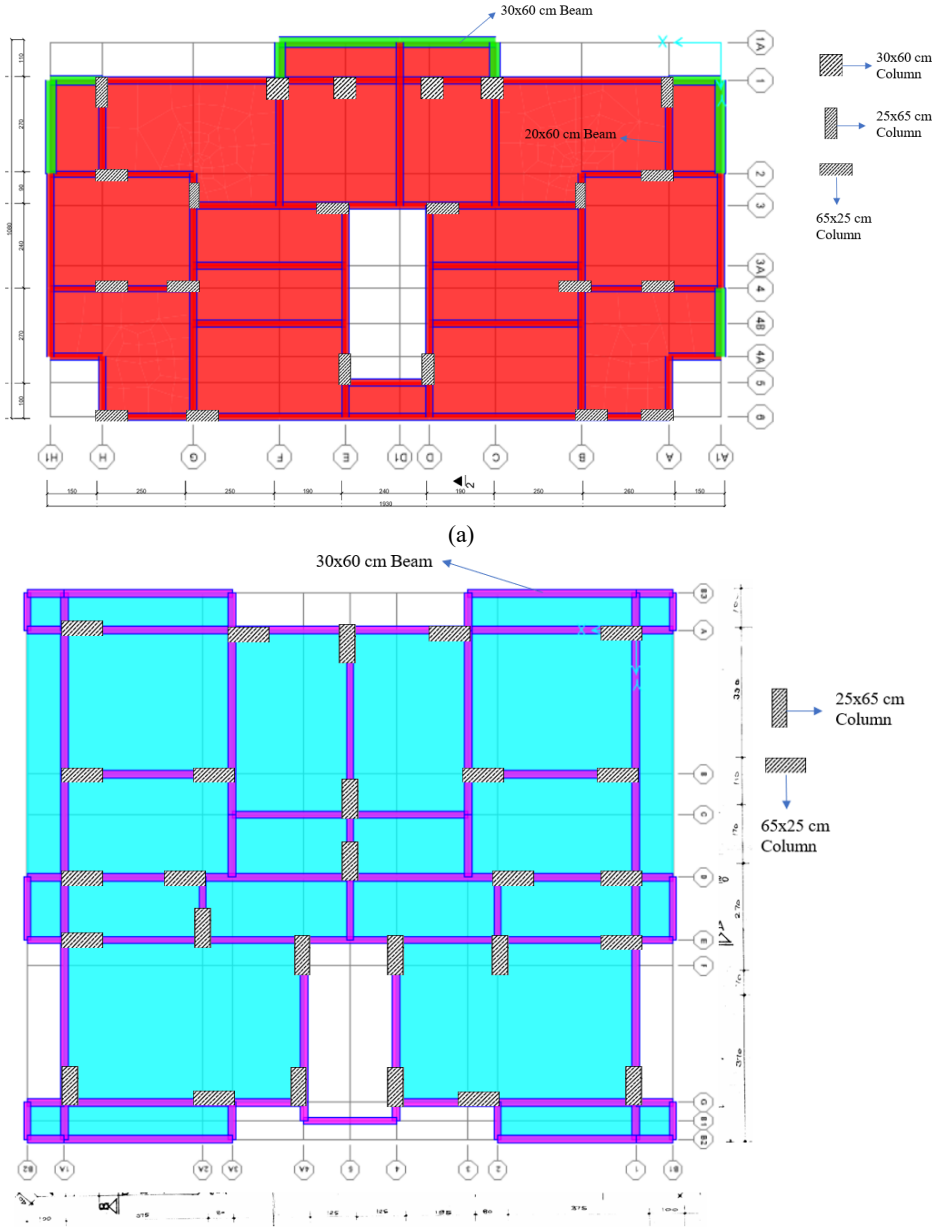


Fig. 1. Formwork plans of the investigated buildings: (a) S1 model, (b) S2 model

The same structural system characteristics and material properties were considered for both building models, and each was defined as a reinforced concrete frame structure, supported on a ground floor and four typical stories. While the overall plan areas and story heights of both models are identical, different plan configurations were adopted in their definition in order to represent several stiffness distributions. Hence, the S1 model was configured to have an elongated and asymmetric plan layout, presenting higher height-to-length and length-to-width ratios; this represents a more slender geometry and increased potential for torsional irregularity when subjected to seismic loading. In this respect, the S2 model was designed to have a more compact, regular, and symmetric plan arrangement, which would result in a more balanced lateral

stiffness in both the principal directions. Several of these geometric differences have been documented to produce changes within the pattern of lateral displacement and torsional demand of buildings during strong motions of the ground [33, 34]. Schematic plan layouts of the S1 and S2 building models are sketched in Fig. 1, where Fig. 1a illustrates the irregular S1 model and Fig. 1b illustrates the regular S2 model.

In all building models, the transverse reinforcement detailing was set up to follow the conventional building procedures of the time, which were set by the 1975 Turkish Earthquake Code. So, stirrup confinement was shown with partially given transverse reinforcement, which was in line with the restricted ductile detailing needs of the time. This state has a direct effect on how ductile and confined the structural members are in sections. It is important to note that the relatively wide stirrup spacing used at the extremities of the columns may lower shear capacity and make it more likely that plastic hinges will form early when the building is shaken. These limitations in detailing should be taken into account when looking at analytical data.

2.2. Ground acceleration parameters according to earthquake codes

The ground acceleration parameters of the collapsed and surviving buildings were determined in accordance with the Turkish Earthquake Codes ABYBHY-1975 and TBEC-2018, and are presented in this section. According to ABYBHY-1975, the effective ground acceleration coefficient (C_0) for the first seismic zone is defined as 0.1 g. For the collapsed building, classified as ZIIIb soil type, the average soil period (T_0) was 0.60 s, while the fundamental periods in the X and Y directions were calculated as 0.30 s and 0.41 s, respectively. In contrast, the corresponding periods for the surviving building were 0.32 s and 0.37 s [5]. Under TBEC-2018, the ZIIIb soil type corresponds to the ZD class, for which the design peak ground acceleration (PGA) is 0.457 g. The short-period spectral acceleration coefficient (S_{DS}), the seconds spectral acceleration coefficient (S_{D1}), and the characteristic soil periods (TA and TB) were obtained from the Turkish Earthquake Hazard Map as 1.15 g, 0.573 g, 0.10 s, and 0.498 s, respectively [33].

Both buildings are assumed to be located at coordinates comparable to the Hatay-Defne strong motion station. The key seismological parameters of the Pazarcık and Elbistan earthquakes recorded at this station are given in Table 2. The maximum horizontal ground accelerations at the building site were found to be 1.38 g for the Pazarcık event and 0.027 g for the Elbistan event. The Pazarcık earthquake generated ground motions approximately 14 times greater than the ABYBHY-1975 design level and nearly 3 times higher than the TBEC-2018 design acceleration. As shown in Table 2, the Elbistan earthquake had almost no significant influence at the Defne site; therefore, the Pazarcık records were adopted as the reference input motion for subsequent analyses and comparisons.

The acceleration time histories of the Pazarcık earthquake recorded at the Defne strong-motion station are illustrated in Fig. 2a for the East–West (DPE) and North–South (DPN) components. The scaled acceleration time series adjusted according to the TBEC-2018 provisions are presented in Fig. 2b. The corresponding elastic acceleration spectra, compared with the target spectrum defined in TBEC-2018 for these buildings, are shown in Fig. 3.

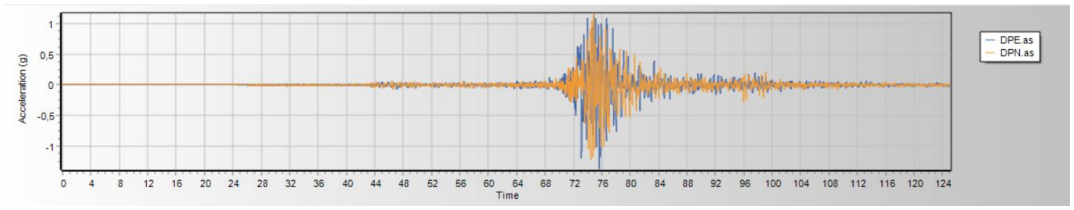
Spectral analysis indicates that the dominant periods of the Pazarcık earthquake are approximately 0.28 s in the East–West (X) direction and 0.25 s in the North–South (Y) direction. Furthermore, the maximum spectral acceleration values obtained from the actual records are 5.3 g and 4.7 g for the East–West and North–South directions, respectively. These values are nearly five times greater than the maximum design spectral acceleration defined by TBEC-2018 for this site, highlighting the significant exceedance of the recorded ground motion over the code-based design spectrum. However, the fact that the dominant periods of the ground motion and the structures differ significantly indicates that the collapse was not triggered by resonance effects. This finding suggests that the structural failure cannot be solely attributed to the intensity of ground acceleration, but is instead influenced by factors such as structural irregularities, stiffness

distribution, and load-transfer mechanisms. In the numerical models, the mass distribution was defined by assigning the tributary mass of each floor to the corresponding story level, including the self-weight of structural members and a portion of the imposed loads in accordance with common practice for seismic analysis. The mass was assumed to be uniformly distributed at each floor level and concentrated at the center of mass of the story.

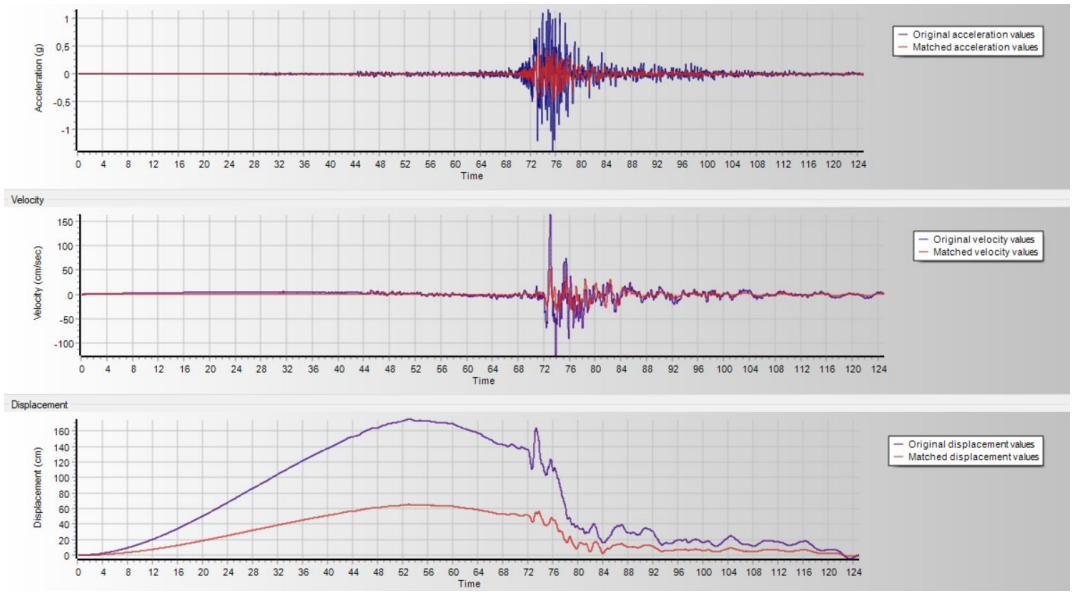
For dynamic analyses, a constant modal damping ratio of 5% was adopted for all modes, representing the inherent damping characteristics of reinforced concrete frame structures. The same damping ratio was used consistently in both modal and linear time-history analyses to ensure compatibility between dynamic properties and response evaluation. These assumptions were maintained for both structural models to allow a consistent comparison of modal periods and dynamic response characteristics.

Table 2. Seismotectonic and strong-motion parameters of the February 6, 2023, Kahramanmaraş earthquakes

Earthquake	Date	Location	Mw	Depth (km)	Latitude (°)	Longitude (°)	PGA (g)	PGV (cm/s)
Pazarcık	February 6, 2023 – 01:17	Kahramanmaraş (Pazarcık)	7.7	8.6	37.288	37.043	1.38	212.94
Elbistan	February 6, 2023 – 10:24	Kahramanmaraş (Elbistan)	7.6	7.0	38.089	37.239	0.027	170.79

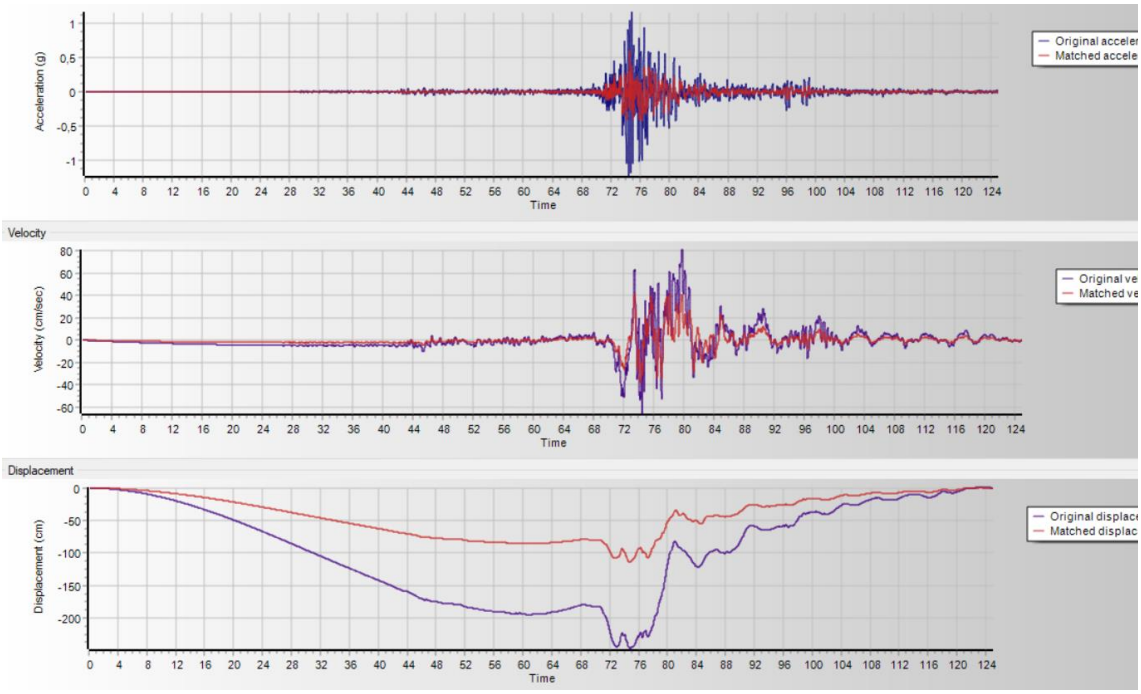


(a)



DPE

Fig. 2. Acceleration – time graphics; (a) original values; (b) matched values



DPN

(b)

Fig. 2. Continued

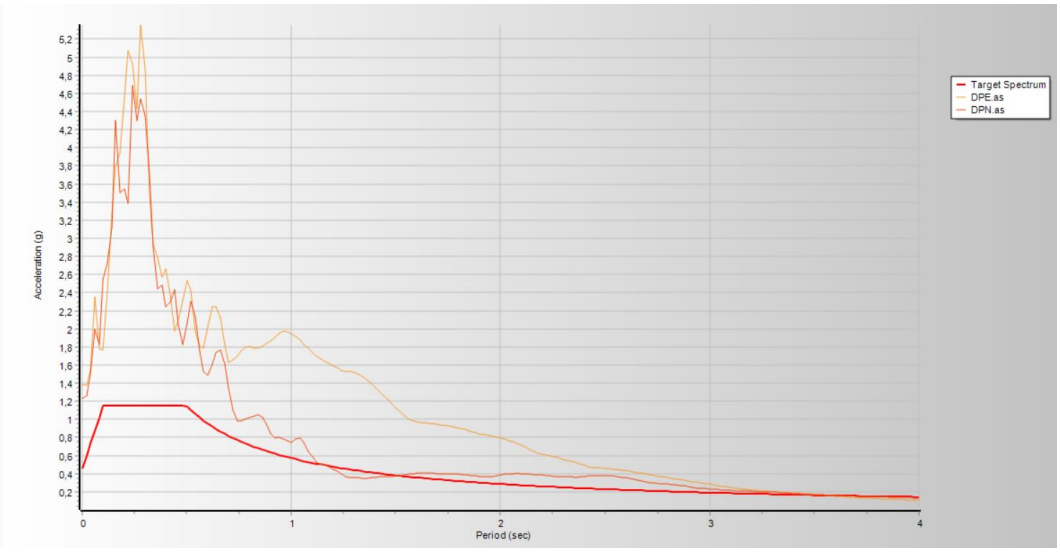
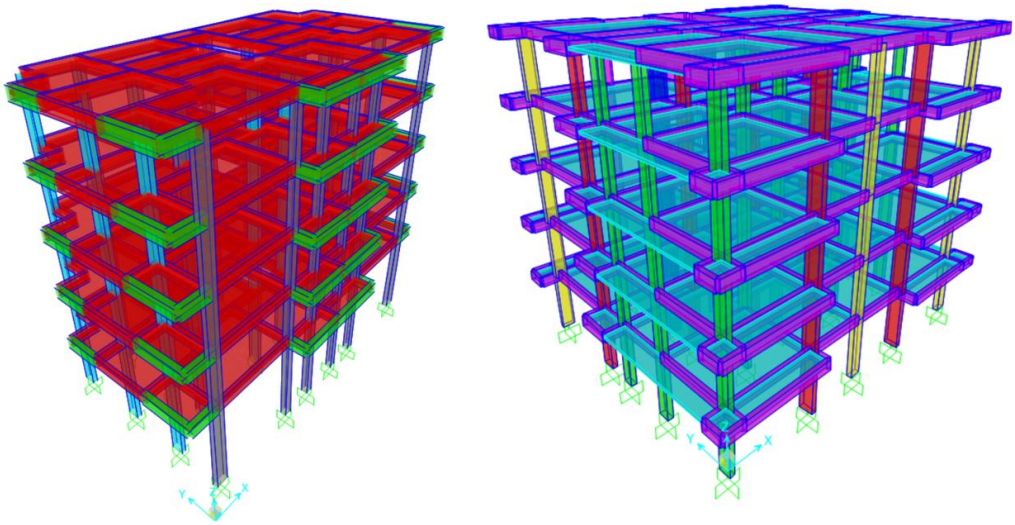


Fig. 3. The component target spectrum and earthquake spectra of the station

2.3. The analysis model and method

The finite element model for the S1 and S2 model buildings was created in the SAP2000 program, as shown in Fig. 4.



(a) (b)

Fig. 4. The finite elements model; (a) S1 model; (b) S2 model

The first calculations for earthquake load were done using the 1975 Turkish Code for the Earthquake-Resistant Design of Buildings (TCERDB 1975). Eq. (1) gives the corresponding static horizontal earthquake loads, Eq. (2) gives the seismic coefficient C, and Eq. (3) gives the structural dynamic coefficient S. T is the structural period, while T_0 is the ground period.

$$F = CW \tag{1}$$

$$C = C_0 KSI \tag{2}$$

$$S = \frac{1}{0.8 + T + T_0} \tag{3}$$

The Turkish Building Earthquake Code 2018 (TBEC 2018) was also used to do the earthquake load analysis. This regulation states that for any level of earthquake ground motion, the ordinates of the horizontal elastic design acceleration spectrum ($S_{ae}(T)$) are given in relation to the acceleration of gravity [g] as a function of the natural vibration period, which is defined in Eq. (4).

$$\begin{aligned} S_{ae}(T) &= \left(0{,}4+0{,}6\frac{T}{T_A}\right) S_{DS}, \quad 0 \le T \le T_A \\ S_{ae}(T) &= S_{DS}, \quad T_A \le T \le T_B \\ S_{ae}(T) &= \frac{S_{D1}}{T}, \quad T_B \le T \le T_L \\ S_{ae}(T) &= \frac{S_{D1} T_L}{T^2}, \quad T_L \le T \end{aligned} \tag{4}$$

where, S_{DS} is the short-period design spectral acceleration coefficient, and S_{D1} is the design spectral acceleration coefficient for a period of 1.0 seconds. There are no dimensions to either of the coefficients. T is the time it takes for something to naturally vibrate. TA and TB are the corners of the horizontal elastic design acceleration spectrum. The Turkish Building Earthquake Code (TBEC 2018) outlines how to compute these factors using Eq. (5).

$$T_A=0{,}2\frac{S_{D1}}{S_{DS}}, \qquad T_B=\frac{S_{D1}}{S_{DS}} \tag{5}$$

Eq. (6) was used to find the Earthquake Load Reduction Coefficient Ra(T), which is utilized to lower the linear elastic earthquake loads according to the Turkish Building Earthquake Code TBEC 2018.

$$R_a(T) = \frac{R}{I} \tag{6}$$

For the earthquake direction (X), we used Eq. (7) from TBEC 2018 to figure out the entire equivalent seismic load that was exerted on the overall structure. This is the same as the base shear force Vte(X).

$$V_{te}^{(X)} = m_t S_{aR}(T_p^{(X)}) \geq 0.04 m_t I S_{DS} g \tag{7}$$

The base shear force in the X-direction is V_{te}, the total structural weight from the G + nQ load combination is mt, and the earthquake load reduction coefficient is S_{aR}. Eq. (8) shows how these numbers were figured out.

$$S_{aR}(T)=\frac{S_{ae}(T)}{R_a(T)} \tag{8}$$

In this study, linear dynamic analyses were performed in the time domain to accurately capture the structural response under real ground motions. A total of 11 ground motion records from different seismic regions of Türkiye were utilized. The essential characteristics of these earthquakes are presented in Table 3. As seen in Table 3, the moment magnitudes (Mw) of the selected earthquakes range between 6.0 and 7.1, while the peak ground accelerations (PGA) vary between 0.064 g and 0.819 g. This range represents moderate to strong ground motions and provides a comprehensive basis for evaluating structural response under varying intensity levels. The selected records were obtained from events such as the 1992 Erzincan, 1999 Düzce, 2003 Bingöl, 2011 Van, and 2020 Sivrice earthquakes—each corresponding to distinct fault mechanisms and site conditions across Türkiye.

Table 3. Characteristics of the earthquake records used in time-history analyses

Earthquake	Abbreviation	Date	Station	Latitude	Longitude	PGA (g)	Magnitude (Mw)
Erzincan	erz	13.03.1992	Erzincan City Center	39.7159	39.6292	0.488	6.6
Düzce	dz	12.11.1999	Bolu City Center	40.806	31.187	0.819	7.1
Afyon (Sultandağı)	af	03.02.2002	Afyon City Center	38.52	31.202	0.115	6.5
Bingöl	bn	05.01.2003	Bingöl City Center	38.9987	40.4637	0.511	6.3
Van	v	23.10.2011	Muradiye	38.689	43.4657	0.191	7.0
Sivrice	sv	24.01.2020	Sivrice	38.3593	39.063	0.298	6.8
Aegean Sea	ed	20.07.2017	Bodrum	36.9198	27.4435	0.161	6.5
Çivril	cv	01.10.1995	Denizli Çivril	38.0561	30.1515	0.327	6.4
Orta	o	06.06.2000	Çankırı Orta	40.7	32.982	0.064	6.0
Sındırgı	sn	27.10.2025	Sındırgı	39.196	28.200	0.380	6.1

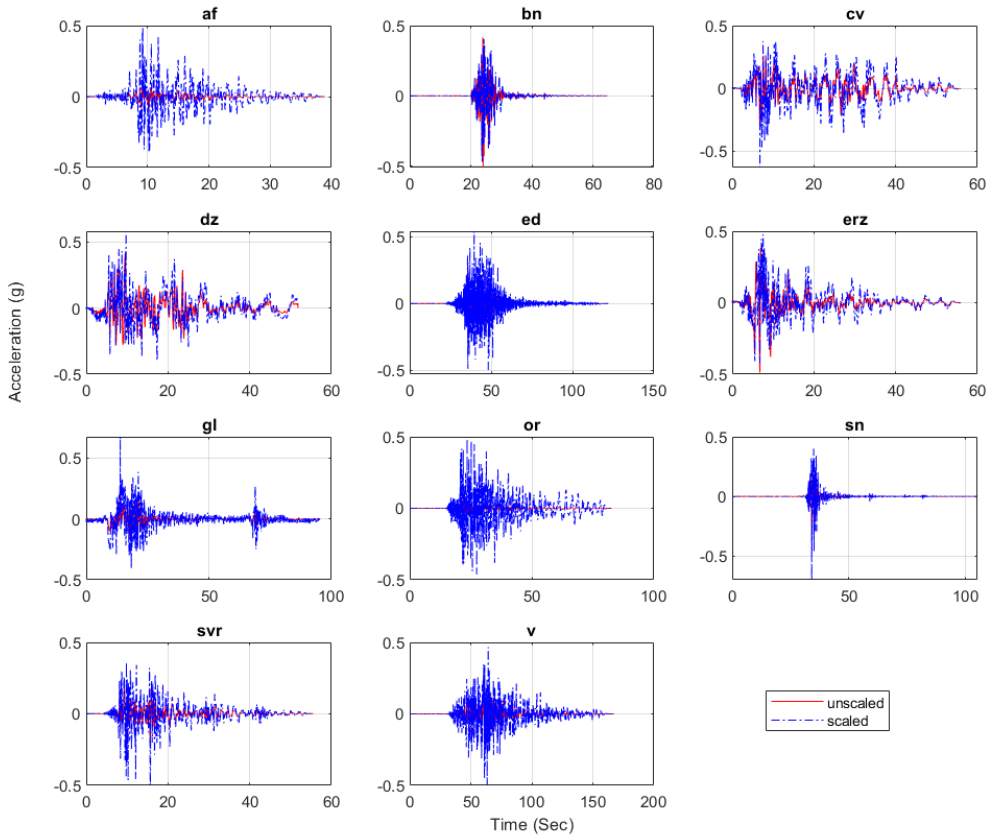


Fig. 5. Unscaled and scaled acceleration–time histories of the selected earthquake records

According to TBEC 2018, the ground motion records employed in time-history analyses must be spectrally scaled to match the design spectrum corresponding to the considered seismic hazard level. Therefore, all selected acceleration records were multiplied by appropriate scale factors to achieve compatibility with the target spectrum defined in TBEC 2018. Fig. 5 presents the comparison between unscaled (red lines) and scaled (blue dashed lines) acceleration-time histories for each record. As illustrated, the scaling process did not alter the overall waveform characteristics of the records; rather, it adjusted only their amplitudes to ensure energy equivalence with the design spectrum. The figure reveals that the Düzce (dz), Erzincan (erz), and Bingöl (bn) earthquakes exhibit high-amplitude, short-duration pulses, typical of near-fault motions, while the Afyon (af), Aegean Sea (ed), and Orta (or) earthquakes display lower-amplitude but longer-duration ground motions. Such diversity allows for the examination of structural behavior under both near- and far-field effects. Following the scaling process, the PGA values of the records were adjusted such that their spectral accelerations collectively align with the target spectrum across the relevant period range. The duration of the scaled motions varies between approximately 40 s and 150 s, encompassing both short- and long-duration events. This variety enhances the robustness of the dynamic response evaluation under multiple ground motion characteristics.

As observed in Fig. 6a, the unscaled spectra differ significantly in spectral acceleration amplitude, particularly within the short-period range (0–1 s). Some motions, such as those from the Düzce and Van earthquakes, exhibit spectral peaks exceeding 1.5 g, while others remain below 0.5 g. After the scaling procedure (Fig. 6b), these discrepancies are considerably reduced, and the spectra converge, especially between 0.2 s and 1.0 s, where structural periods of interest generally lie. The comparison in Fig. 6c

demonstrates that the mean scaled spectrum shows excellent agreement with the TBEC 2018 target design spectrum. The scaled spectra closely follow the target curve within the short- and medium-period range (0.1–1.0 s), and deviations at longer periods are minimal. This confirms that the scaling process effectively ensured spectral compatibility and that the selected ground motion set statistically represents the design-level seismic demand prescribed by TBEC 2018. Overall, the adopted scaling methodology ensures that both the amplitude and frequency content of the ground motions are consistent with the target seismic hazard. Consequently, the time-history analyses conducted using these records provide reliable and code-compliant assessments of the structural seismic performance.

Given that the spectral compatibility of the selected ground motion records is already established, as shown in Fig. 6, the next step involves setting the reference limits within which the analytical results from the S1 and S2 models will be compared. Under these premises, the required stresses, shear forces, interstory drifts, floor accelerations, and dynamic characteristics obtained from the analyses are interpreted in view of design provisions and material limits according to the 1975 Earthquake Code, TBEC 2018, TS 500, and other international relevant standards. To provide a clear basis for such comparisons, Table 4 provides the fundamental limit values for C14 concrete and S220 reinforcement: allowable compressive and tensile stresses, shear stress capacity, drift limits, and typical period ranges. These will form the reference framework through which the seismic performance of both building models is assessed in subsequent sections.

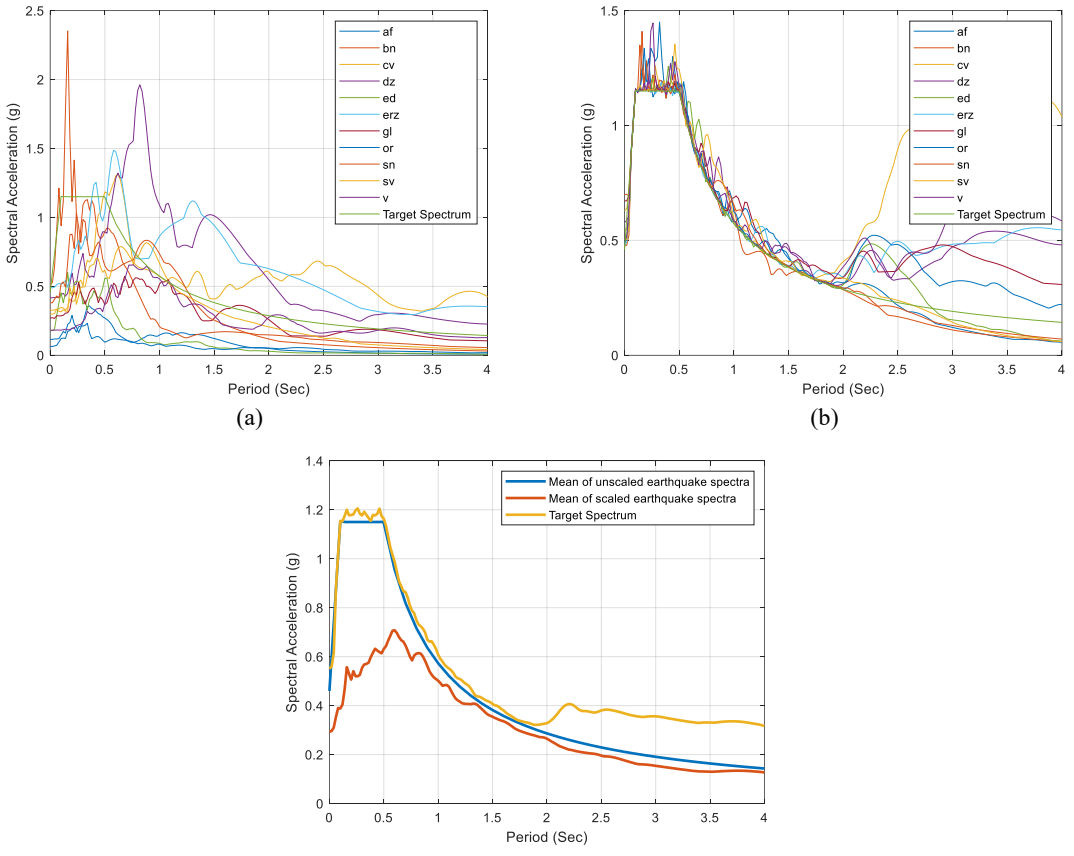


Fig. 6. Response spectra of the selected earthquake records and comparison with the TBEC 2018 target spectrum; (a) Unscaled earthquake spectra, (b) Scaled earthquake spectra, (c) Mean spectra of unscaled and scaled records

Table 4. Limit values for RC members with C14 concrete and S220 reinforcement according to the 1975 Code, TBEC 2018, and international standards

Parameter	1975 Earthquake Code TS 500 [5]	TBEC 2018 TS 500 [2]	International Standards [33]–[36]	Explanation
Concrete compressive strength	fck = 14 MPa	fcd = fck/1.5 ≈ 9.3 MPa	EC2 [34]: fcd = fck/1.5	Design compressive strength
Characteristic tensile strength	ft ≈ 0.33√fck ≈ 1.2 MPa	fctm ≈ 1.2 MPa	EC2 [34]: fctm ≈ 1.2 MPa	Cracking stress limit
Rebar yield strength (S220)	fyk = 220 MPa	fyd ≈ 191 MPa	—	Yield strength of reinforcing steel
Allowable shear stress (τ)	0.7–0.8 MPa	vRd ≈ 0.7–1.0 MPa	EC2 [34], ASCE 41 [33]: 0.6–1.2 MPa	Critical shear stress range
Interstory drift ratio (θ)	Not specified	0.008 rad (LS), 0.004 rad (IO)	ASCE 41 [33], FEMA 356 [35], [37]: 0.01 rad	Drift performance limits
Beam deflection limit	Not defined	L/250 – L/200	EC2 [34]: L/250 – L/200	Serviceability limit
Critical floor acceleration	Not defined	No direct limit	FEMA 356 [35], ASCE 41 [33]: 0.3–0.5 g	Non-structural component demand
Typical period range (3–5 story RC frames)	T ≈ 0.3–0.7 s	T ≈ 0.3–0.8 s	ASCE 7 [36]	Expected dynamic range

Table 4 summarizes the basic mechanical and seismic performance limits used to interpret the analytical results of the S1 and S2 models. Herein, fck is the characteristic compressive strength of concrete; fcd represents the corresponding design strength as defined in ABYBHY-1975 [5] and TS 500. Tensile strength values, ft and fctm, prescribe the cracking stress levels where stiffness degradation starts. Yield strength parameters of S220 reinforcement, fyk and fyd, represent the elastic limit of reinforcing steel. Shear stress limits τ are obtained from the 1975 Code [5], TBEC 2018 [2], and international standards such as Eurocode 2 (EC2) [34] and ASCE 41 [33]. Interstory drift limits are introduced according to TBEC 2018 provisions as 0.008 rad for Life Safety and 0.004 rad for Immediate Occupancy, while the widely accepted upper drift limit of 0.01 rad, supported by both ASCE 41 [33], FEMA 356 [35], and the well-established RC seismic design literature of Paulay and Priestley [37], was adopted as the literature-based reference. Beam deflection limits within the range L/250–L/200 are identical to TS 500 and EC2 [34]. Floor acceleration thresholds between 0.3 and 0.5 g come from FEMA 356 [35] and ASCE 41 [33]. The expected structural period ranges for low-rise RC moment-resisting frames between 0.3 and 0.8 s are consistent with the recommendations of ASCE 7 [36]. These limits will constitute the reference framework in the subsequent sections while interpreting the seismic performance of the S1 and S2 models.

The inquiries in this study were conducted inside the linear elastic framework. This technique was deliberately selected to align with the design concepts of the 1975 Turkish Earthquake Code, which does not account for nonlinear material behavior or the formation of plastic hinges. As a result, the results are looked at in terms of seismic demand indicators instead of predicting ultimate capacity or collapse.

In this study, all structural models were analyzed based on the premise of fixed-base conditions. Soil–structure interaction effects were intentionally omitted to concentrate on the influence of ground acceleration intensity and structural configuration on seismic demand parameters. While SSI might affect spectral amplification and drift dispersion, particularly in soft soil conditions, its analysis is beyond the scope of this work. As a result, the data are studied in a comparative way instead of as final response predictions.

A frequency-domain study was also done to examine more closely how the structural responses change over time. You frequently need to utilize filtering and windowing procedures when you work with recordings of ground motion that were taken in the field. In this investigation, FFT analysis was directly utilized on the structural acceleration responses obtained from numerical calculations rather than from unprocessed field measurements. So, only baseline correction was done before the frequency-domain analysis, and no extra filtering or windowing was done to keep the original structural frequency content. We use the FFT data as supplementary signals to help us locate the main frequency trends in the structural response. They are not the best approach to judge how well someone is doing.

3. Evaluation of analysis results

Dynamic properties and seismic response of the S1 and S2 models are evaluated in this section by modal analysis, equivalent seismic load procedures, linear time-history analyses, and recorded ground motion. Assessment of modal behavior is followed by a comparative assessment of base shear forces, displacement and acceleration demands, stress distributions, and interstory drift ratios subject to seismic effects. The fundamental periods and modal mass participation ratios obtained from the modal analysis are summarized in Table 5. From these results, it can be seen that the first-mode period is determined as 0.761 s for Model S1, and as 0.518 s for Model S2, indicating that S1 has a lower global stiffness value than S2. For both models, more than 97% mass participation is reached in the first three modes in the horizontal directions, which satisfies the minimum modal participation recommended by both ASCE 7 and ASCE 41 [33, 36]. Torsional mass participation ratios were determined as 2.57% and 6.30% for S1 and S2, respectively, which implies that the torsional mode contributes only marginally to the dynamic response in both structures. These modal analysis results will form a basis for interpreting subsequent results on base shear forces, roof displacements, acceleration demands, and stress distributions.

The first three mode forms from the modal analysis, which are shown in Fig. 7, are used to compare the dynamic behavior of both structural configurations even more. The investigations of these mode forms reveal that, in both S1 and S2 models, the first mode is characterized by lateral deformation in one horizontal direction, the second mode arises from lateral deformation in the orthogonal direction, and the third mode is associated with torsional vibration. The distorted patterns of the first and second modes in the S1 model show larger displacement shapes, which match the longer period values in Table 5. The S2 variant, on the other hand, has a more compact profile since it is stiffer and has shorter modal periods. The torsional contribution recorded at the third mode is still modest for both models. This is in line with the low torsional mass participation ratios shown in Table 5. These traits are a key part of understanding the conclusions of the analysis that follows, which includes base shear forces, roof displacements, and interstory drift ratios.

Table 5. Fundamental periods and modal mass participation ratios of the S1 and S2 models

Models	T_1 (s)	T_2 (sec)	T_3 (s)	Mass ratio Ux (%)	Mass ratio Uy (%)	Mass ratio Uz (%)
S1	0.761	0.695	0.649	99.95	99.94	2.57
S2	0.518	0.452	0.438	99.18	97.53	6.30

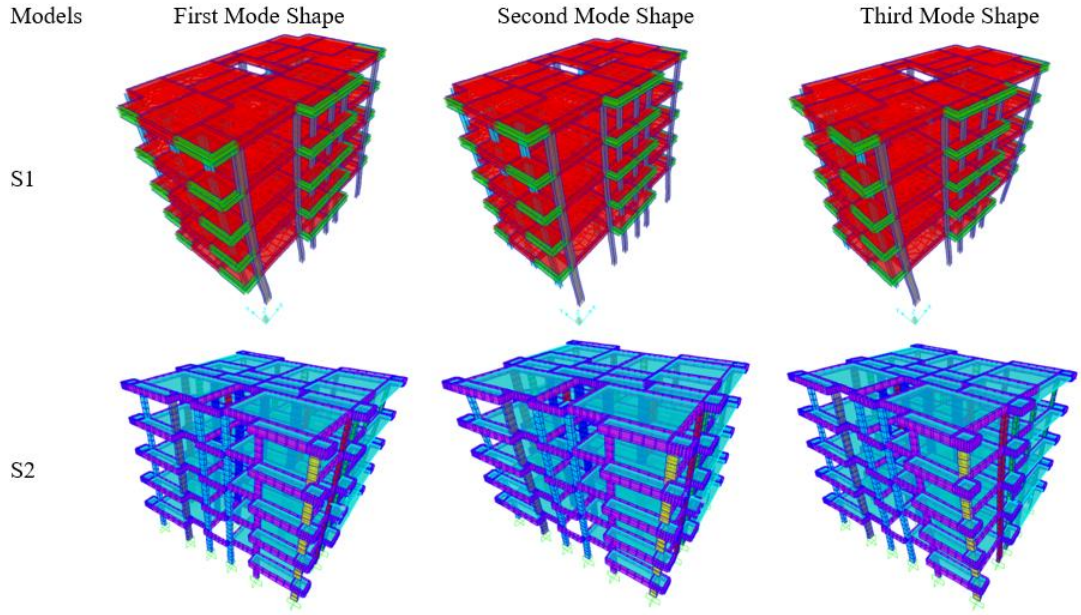


Fig. 7. A comparison of the first three mode forms for the S1 and S2 models

Table 6. Base shear forces, roof displacement values, and roof acceleration demands of the S1 and S2 models under different seismic loading procedures

Earthquake	Models	Base shear force (kN)	Roof displacement (m)	Roof acceleration (g)
Afyon (af)	S1	2390	0.0713	0.93
	S2	3154	0.0550	1.36
Bingöl (bn)	S1	1817	0.0652	0.77
	S2	3018	0.0579	1.13
Çivril (cv)	S1	2232	0.0671	0.65
	S2	3139	0.0565	1.07
Düzce (dz)	S1	2018	0.0798	0.86
	S2	3281	0.0576	1.18
Ege Denizi (ed)	S1	2334	0.0616	0.69
	S2	3159	0.0552	1.06
Erzincan (erz)	S1	2418	0.0691	0.96
	S2	5479	0.109	1.79
Gölcük (gl)	S1	2423	0.0714	0.73
	S2	3367	0.0682	1.16
Orta (or)	S1	2471	0.0699	0.87
	S2	3025	0.0521	1.37
Sındırgı (sn)	S1	1818	0.0706	0.91
	S2	3003	0.0612	1.08
Sivrice (sv)	S1	2455	0.0705	0.81
	S2	3299	0.0520	1.22
Van (v)	S1	2659	0.0791	0.71
	S2	5251	0.113	1.78
Mean Earthquake (m)	S1	2275	0.0705	0.81
	S2	3561	0.0670	1.29
Defne (Dpe)	S1	6433	0.178	2.07
	S2	8060	0.171	3.18

To evaluate how the S1 and S2 models reacted to earthquakes with different loading methods, we looked at the base shear forces and roof displacements from different assessments side by side. Both models produced comparable base shear forces under the Ex-1975 and Ey-1975 loading conditions established by the 1975 Earthquake Code; however, the S2 model exhibited reduced roof displacements owing to its increased stiffness. TBEC 2018 described the Ex-2018 and Ey-2018 loading situations. The S1 model had much bigger displacement demands, especially in the Ey-2018 direction. The S2 model produced higher base shear values, but the S1 model achieved greater roof displacement levels in the average time-history response ("Time History (m)"). When tested with the real Defne (Dpe) ground motion from the Pazarcık earthquake, both models showed much higher seismic demands. The base shear values went up to 6433 kN for S1 and 8060 kN for S2, and the roof displacements were 0.178 m and 0.171 m, respectively. These results indicate that actual ground vibrations may exert considerably greater demands than code-based seismic loading methodologies.

Among the seismic loading cases presented in Table 6, Fig. 8 includes only the base shear and roof displacement values obtained from the average time-history analysis (Time History (m)) and the actual Defne (Dpe) ground-motion record. In addition, to assess the comparative effect of code-based seismic actions, Ex-1975, Ey-1975, Ex-2018, and Ey-2018 loading cases were also plotted. In this context, Ex-1975 and Ey-1975 denote the horizontal seismic forces calculated in the X- and Y-directions, respectively, considering the Equivalent Seismic Load Method presented in the 1975 Earthquake Code. Similarly, Ex-2018 and Ey-2018 represent the seismic load effects obtained in the X- and Y-directions based on the Equivalent Seismic Load Method presented in the Turkish Building Earthquake Code, TBEC 2018. Thus, seismic demands obtained from historical and modern code provisions in 1975 and 2018, respectively, as well as those obtained from the real ground motion record and mean time-history response, are presented comparatively in a single figure, enabling a comprehensive assessment of the influence of different analysis methodologies on the structural response.

Fig. 9 shows the stress contour plots for the compressive and tensile stress distributions obtained in S1 and S2 models under the G+0.3Q, G+0.3Q+Ex/Ey (1975), and G+0.3Q+Ex/Ey (2018) load combinations. Under the gravity load case G+0.3Q, both models develop relatively uniform stress distributions; however, higher compressive and tensile demands are observed in slab-beam connections and lower-story columns of the S1 model. When seismic effects are introduced by the G+0.3Q+Ex/Ey (1975) and G+0.3Q+Ex/Ey (2018) combinations, the tendency of stress concentration in S1 becomes more pronounced at the frame corners and ground-story columns, where both compressive and tensile demands strongly increase. When the color scales are considered, various regions in S1 develop compressive stresses that definitely exceed the design compressive strength of C14 concrete ($f_{cd} \approx 9.3$ MPa) and tensile stresses approaching or surpassing the characteristic tensile strength ($f_t \approx 1.2$ MPa) provided in Table 4. Indeed, this would mean higher chances of early cracking, stiffness degradation, and plastic hinge formation in S1. In contrast, S2 exhibits a more uniform and moderate stress distribution in which both compressive and tensile demands are kept below the values developed in S1 for the same set of load combinations and remain generally closer to, or below, the limit values summarized in Table 5. The difference between the two models clearly becomes evident when the G+0.3Q+Ex/Ey (2018) combinations defined by TBEC 2018 are considered; the stiff and regular structural configuration of S2 makes seismic forces distribute more evenly, thus limiting sectional stress demands. Based on these observations, despite having similar material properties, the S1 model is much more prone to exceed safe stress ranges expected for a C14-S220 system, whereas S2 maintains a comparatively safer state of stress under the same conditions of seismic loading.

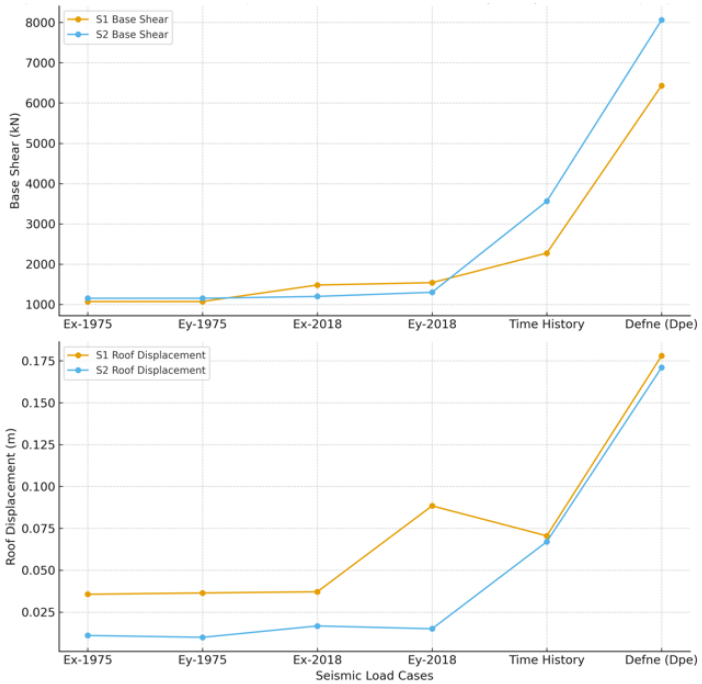


Fig. 8. Variation of base shear and roof displacement for S1 and S2 models under different seismic loading procedures

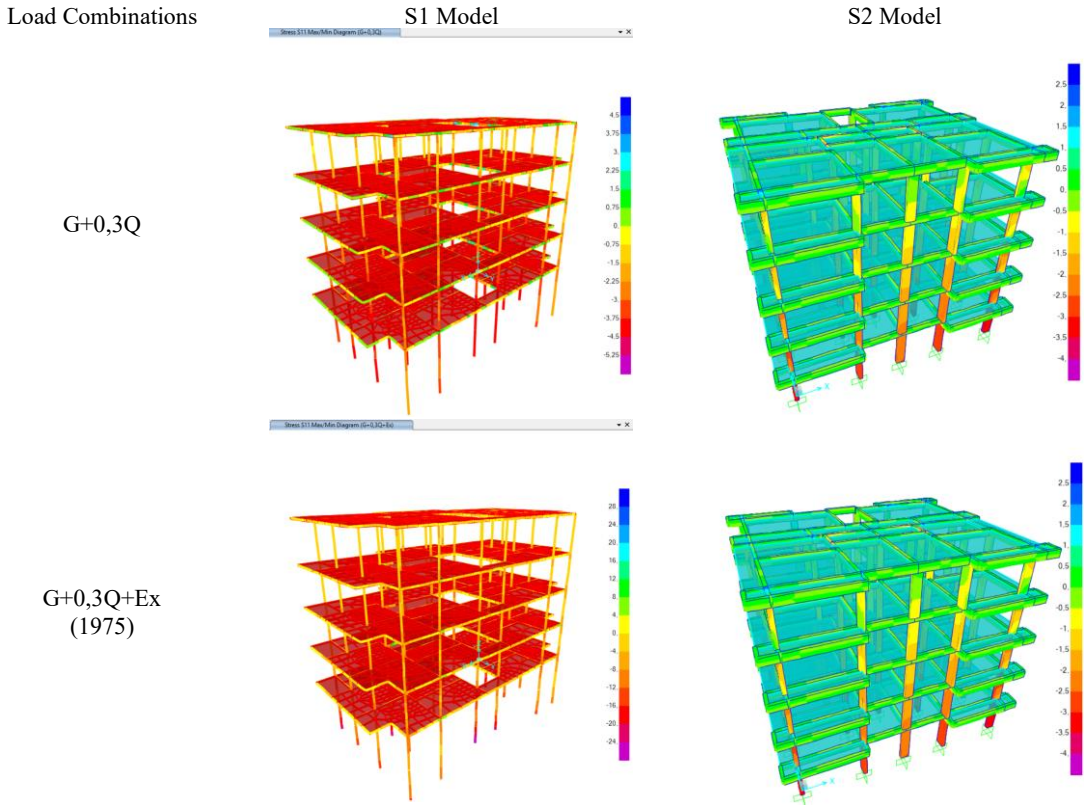


Fig. 9. A look at how compressive and tensile stress are spread out in S1 and S2 for different load combinations

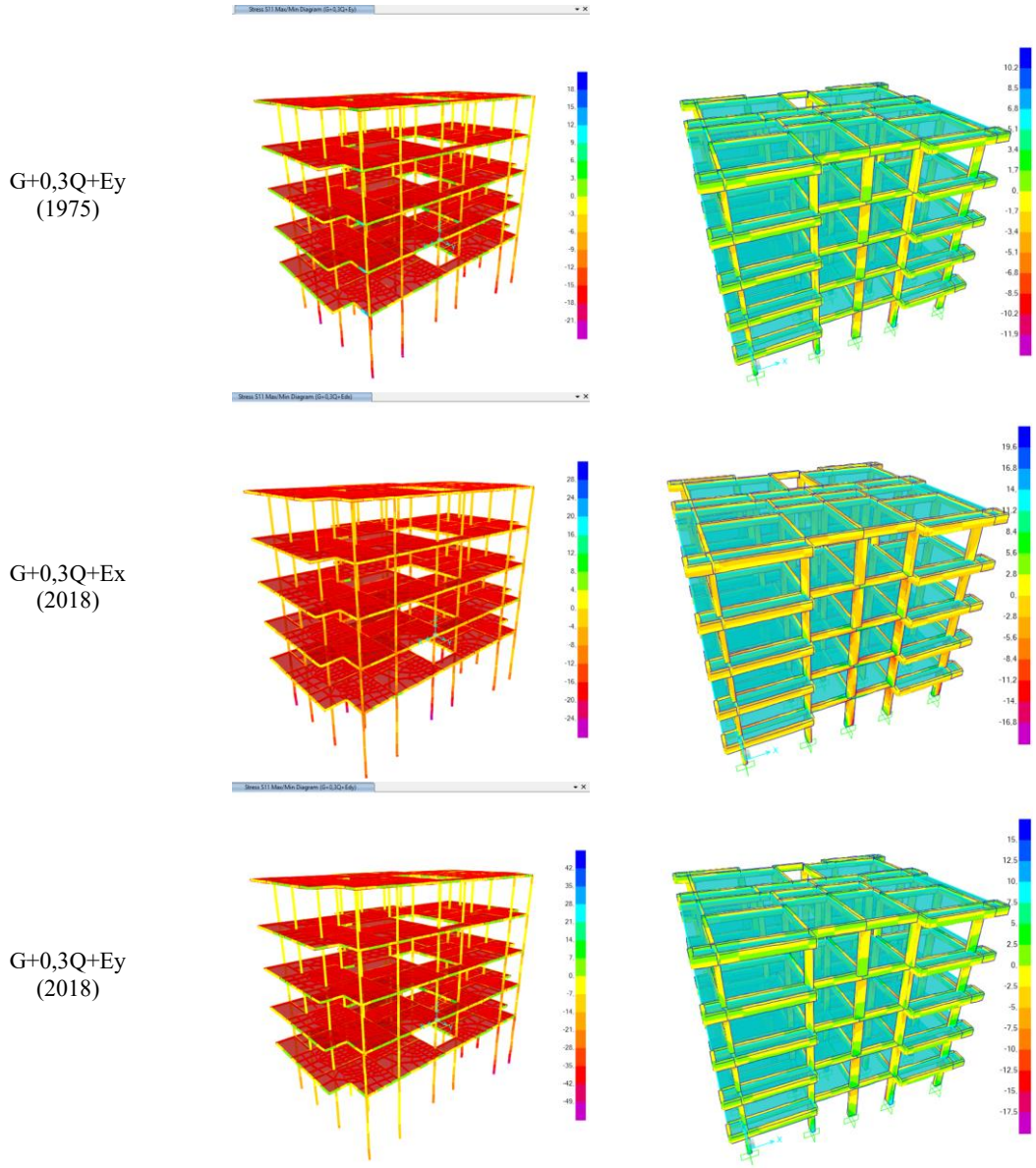


Fig. 9. Continued

The shear stress distributions derived from the examined load combinations elucidate the sectional shear demand in the S1 and S2 structural models. Under G+0.3Q loading, both models have very modest shear stresses. However, there are obvious stress concentrations at the ground-story column–beam joints of S1. This is because this area is more sensitive to shear effects caused by gravity. When seismic loads are added to the G+0.3Q+Ex/Ey (1975) combinations, the resulting shear patterns show the same seismic loading method that was laid out in the 1975 Earthquake Code [5]. However, S1 shows more pronounced shear concentrations because of the structural irregularities it carries. Finally, the shear stress distributions from the G+0.3Q+Ex/Ey (2018) combinations meet the requirements of TBEC 2018 [2]. S1, on the other hand, has significant shear demands at the corner columns, around the stair core, and in the outermost frame elements. Conversely, S2 exhibits a markedly more uniform distribution of the increasing stresses,

characterized by significantly reduced peak values. Table 4 shows that the limit values of shear stresses for C14 concrete are in line with the relationships given in many international codes and stress models that are commonly used [33–35]. For S1, various combinations produce shear stresses that are near or even over this threshold in the G+0.3Q+Ex (1975) and G+0.3Q+Ey (2018) combinations. The resulting shear demands show that the system is more likely to respond in a shear-critical way. This conclusion is consistent with other research indicating an elevated likelihood of shear failure in low-strength and irregularly reinforced concrete structures [36, 37].

In the context of the Time History (m) loading, which represents the average response of the chosen ground motions, the S1 model generates shear stress levels—particularly around the stair-core area—that are similar to or slightly lower than those of the critical 1975–2018 code-based combinations. Some portions get close to the design shear strength τ, and comparable behavior has been linked to possible brittle shear response in the literature [33–36]. The S2 model keeps shear levels reasonable, with the highest values in important areas well below the limit (Fig. 10). The difference between these two models becomes significantly bigger when they are compared to the Defne Dpe ground-motion data. In S1, many columns and beam ends on the ground floor, close to the cantilever areas, meet or surpass their τ limit (Fig.10). This is in line with the fact that shear demand goes up a lot when the shaking is substantial. These exceedances have been demonstrated to cause shear-dominated failures in low-strength or seismically weak RC buildings [36, 37]. The maximum stresses in the S2 model also go up under Dpe, but they stay well below the limit. The critical areas are only in tiny areas, hence the S2 model is better at resisting shear than the S1 model.

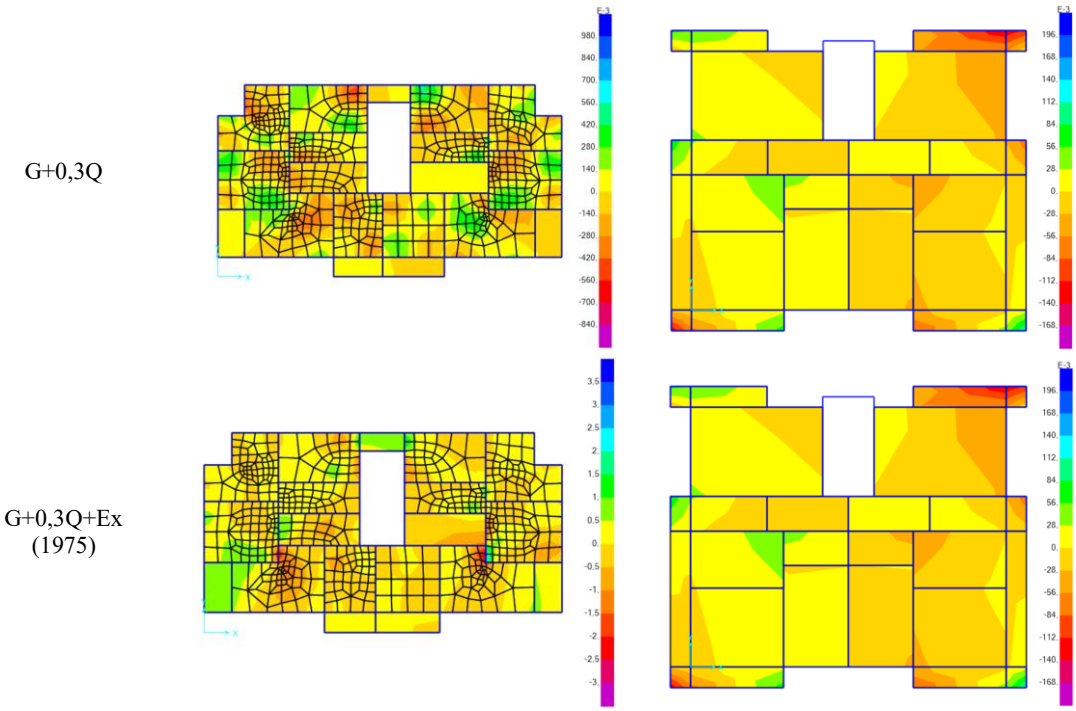


Fig. 10. Comparison of shear stress distributions in the S1 and S2 models under various load combinations

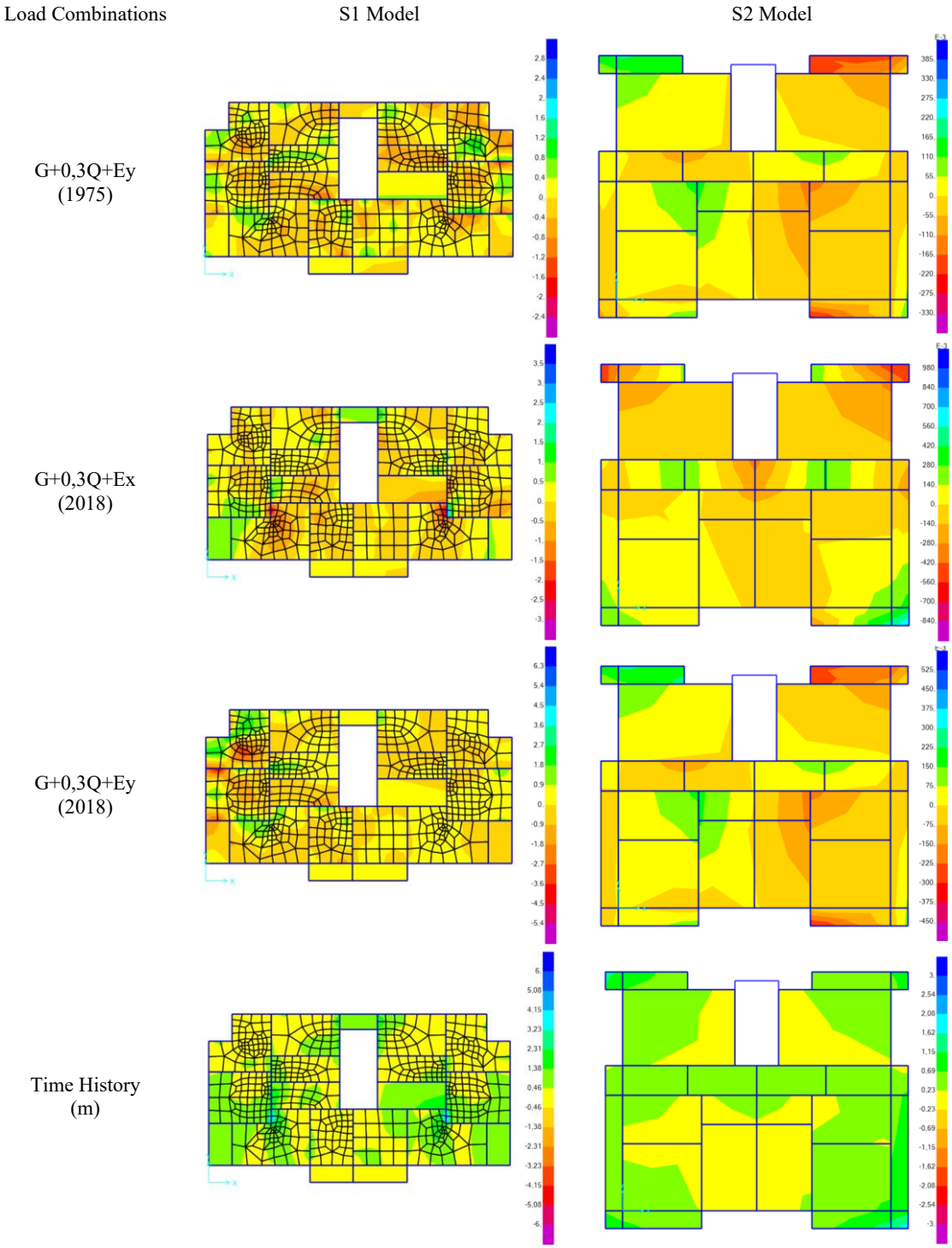


Fig. 10. Continued

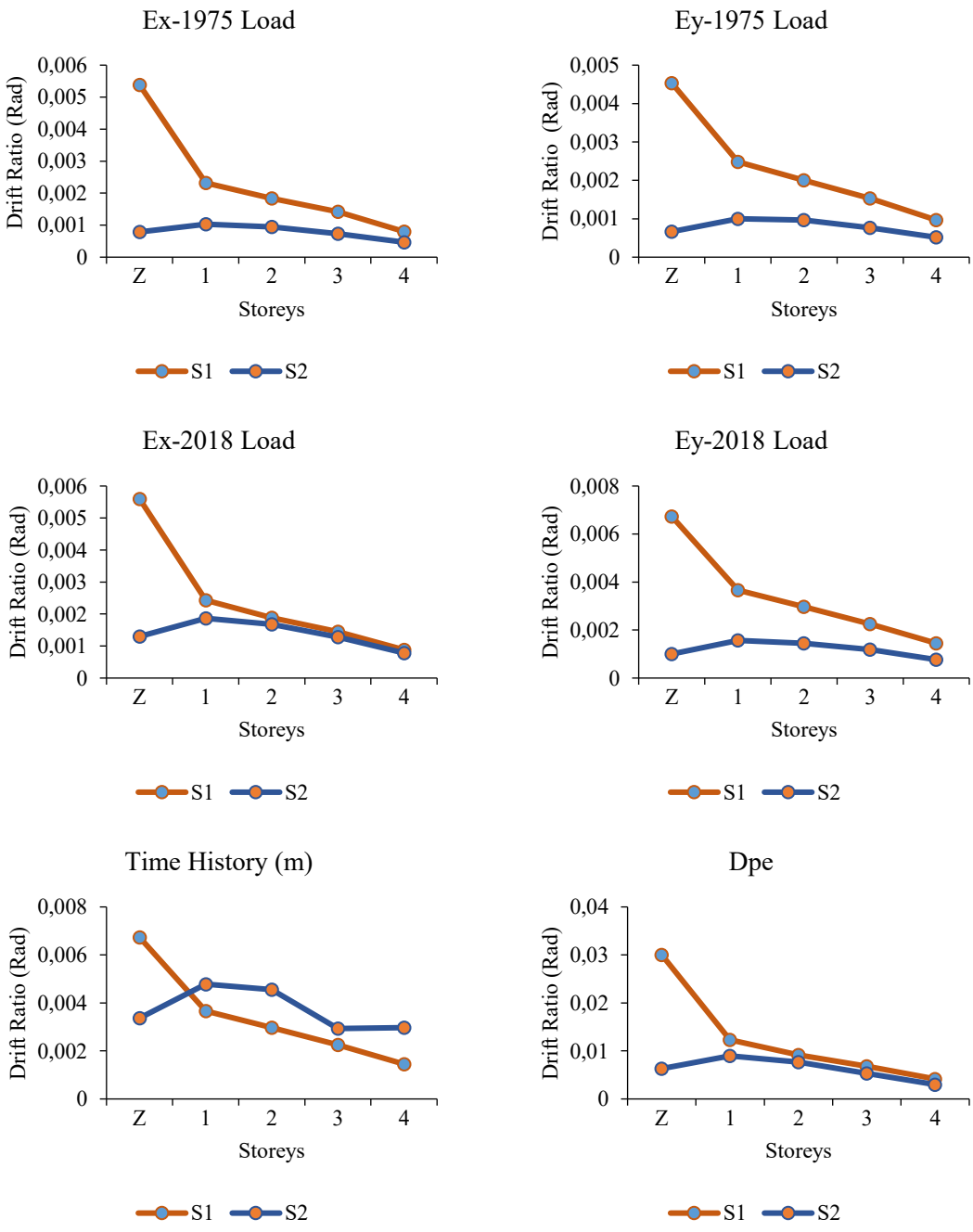


Fig. 11. Interstorey drift ratios of S1 and S2 models under various seismic loading scenarios (1975 Code, 2018 Code, Time History, and DPE Record)

Fig. 11 shows the interstory drift ratios for the S1 and S2 models under all of the seismic loading conditions we looked at. These conditions include the equivalent lateral loads defined in the 1975 and 2018 Turkish Earthquake Codes (Ex–Ey 1975 and Ex–Ey 2018), the mean ground motion used in the linear time-history analysis (time history–m), and the actual Pazarcık earthquake record we got in Defne (Dpe). The data are analyzed comparatively to emphasize relative drift demand trends instead of absolute performance classification. The drift profiles show that the 2018 code generally has larger drift demands than the 1975 code. This is because the new regulation calls for higher design spectral accelerations. For the S1 model, the drift ratios for both the 1975 and 2018 corresponding static load situations are about 0.005 to 0.007 rad at the lower floors and get smaller as you go up. The S2 model, on the other hand, has slightly greater but more evenly spread drift requirements, which range from about 0.008 to 0.015 rad along the height of the building. The time-history (m) loading causes the two structural configurations to have very different drift distributions. The S1 model has relatively low drift demands that go down as the height goes up. The S2 model, on the other hand, has a localized increase in drift on the first and second floors before going down as the height goes up. This means that the stiffness is more evenly distributed along the height. The Dpe record shows the biggest variances between the two models. The S1 model's peak drift requirement at the ground level is about 0.030 rad, and it quickly drops in the upper levels, showing a clear soft-storey-type response. The S2 model, on the other hand, has much lower and more evenly spread drift requirements, at 0.006–0.009 rad in the lower levels. This shows a more stable deformation pattern when the earthquake actually happens.

It should be emphasized that slab deflection results are presented as supplementary response parameters and do not represent failure criteria, particularly since no A2 or A3 plan irregularities are present in the investigated models. Fig. 12 shows the UZ-direction deflection distributions, which give a thorough look at how both structures change shape vertically when different loads are applied. When we look at the effects of the 1975 and 2018 seismic codes, as well as time-history studies (Time History) and the recorded Defne motion (Dpe), we can see that the S1 model has far bigger slab deflections. Table 4 shows that several of these peak deflection values are higher than what is allowed by international guidelines. For example, ACI 318-19 [33], Eurocode 2 [34], and TBEC 2018 [2] usually set serviceability limitations between L/250 and L/500. The highest UZ-direction displacements of the S1 model come close to or exceed these restrictions, which shows that the serviceability performance is very important. The S2 model, on the other hand, shows far lower slab deflections, both on average and at their highest points, and stays within the expected standard limits. This behavior can be explained by its more regular structure, more even stiffness distribution, and superior ability to keep deformation balanced when there is seismic loading. The S2 model shows a uniform deflection pattern across all floor levels, especially when G+0.3Q, Ex-2018, and Ey-2018 are combined. The S1 model, on the other hand, shows localized soft-slab behavior at some levels. When the Time History (m) and Dpe results are looked at simultaneously, the S1 model shows greater vertical deflection gradients and localized deflection accumulation under the true earthquake record. This discovery aligns with existing literature indicating that irregular and non-retrofitted structures are prone to substantial vertical deformation during intense ground movements [35–37]. The S2 model, on the other hand, keeps the deflection levels under both the average and real ground motions under control, which makes the transitions from floor to floor smoother. Overall, the way the S1 model bends in the UZ direction shows that it doesn't meet the limit values set by key seismic design and serviceability standards, which shows that it is structurally weak. The S2 model, on the other hand, keeps UZ deflection levels within acceptable limits. This shows that it has a more stable structural response and is good enough for serviceability under seismic stress.

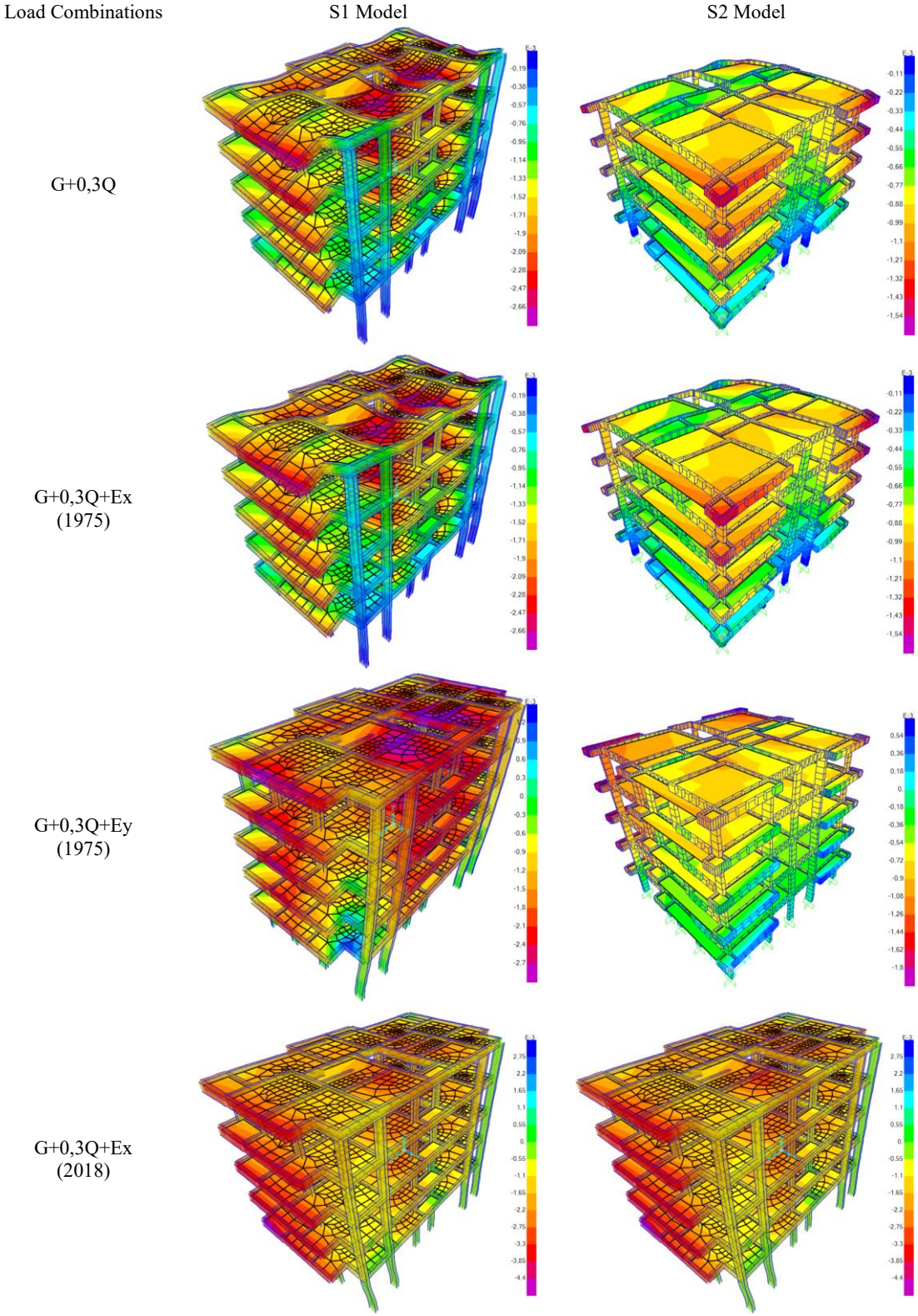


Fig. 12. UZ-direction deflection distributions of the S1 and S2 models under different load combinations

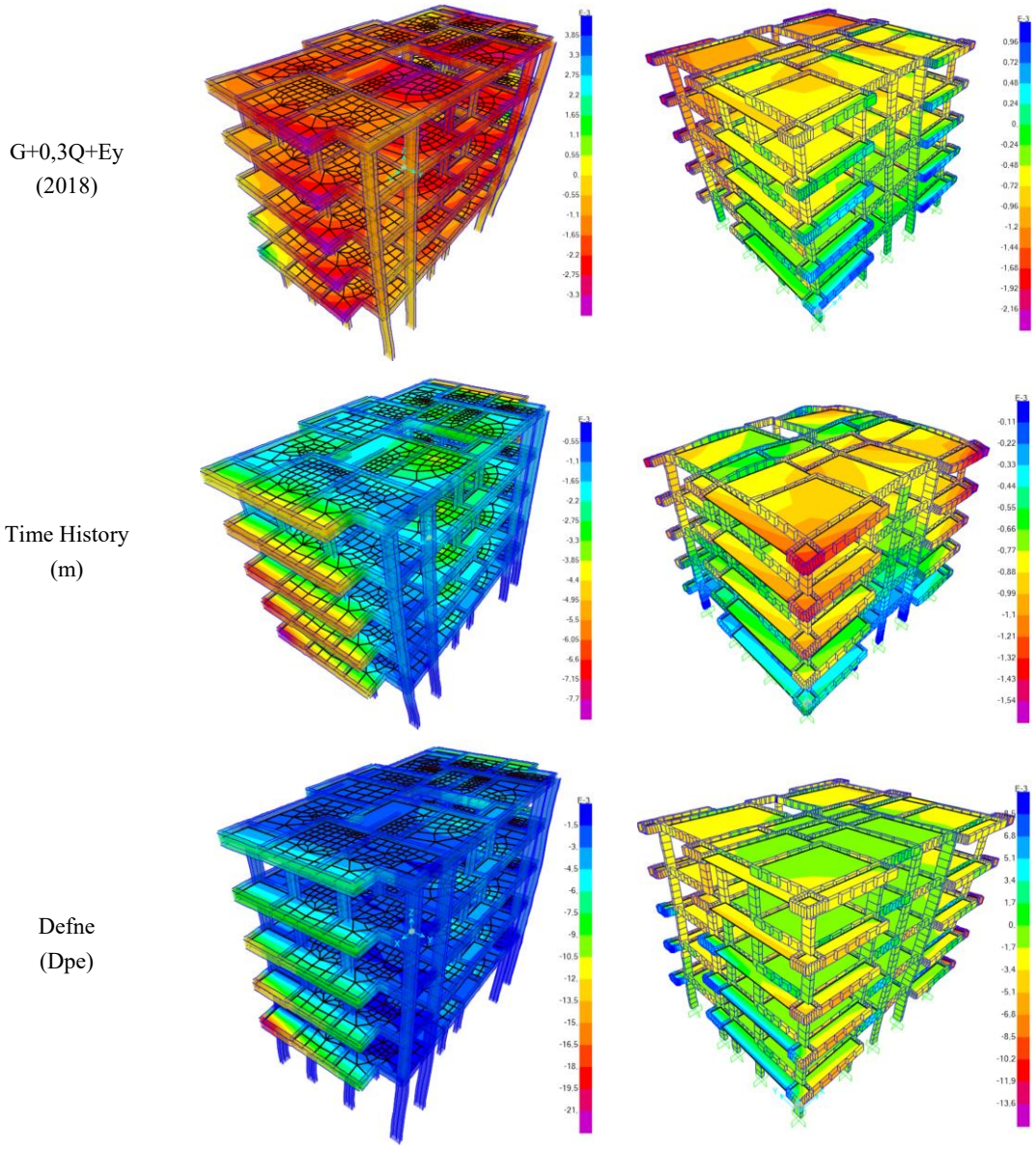


Fig. 12. Continued

Time-history floor acceleration responses obtained from the Dpe (Defne) record are presented in Fig. 13. It is seen that peak acceleration alone cannot be used to infer structural damage. Although the maximum accelerations at all storeys are higher for S2, it was seen earlier that the S1 model exhibits larger interstorey drifts, higher shear stresses, and greater tensile compressive demands. The story-wise acceleration distributions show how the two structural systems alter as time goes on. In the S1 model, the floor accelerations go up steadily from the ground to the ceiling. This means that the first vibration mode is the most essential one. The S2 model, on the other hand, exhibits bigger accelerations up to the third level, followed by a minor dip near the roof. This means that stronger vibration modes are at work because the

setup is stiffer and more regular. The differences are even more obvious when you look at the ratios of amplification from the ground to the roof. The ratio is roughly 1.27 for the S1 model and more than 2.2 for the S2 model. The S2 model has more acceleration amplification along the height, while the S1 model has less acceleration but more reaction quantities linked to drift and displacement.

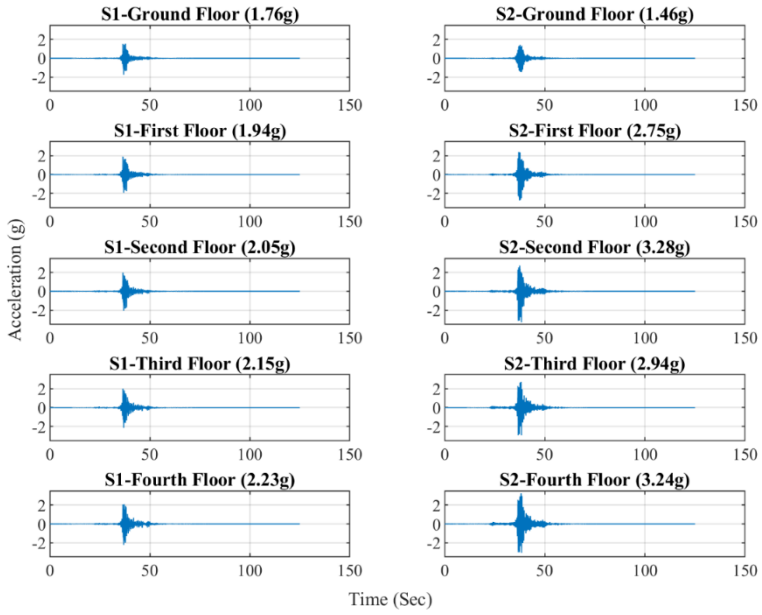


Fig. 13. Storey-level maximum acceleration time-history responses for S1 and S2 models (Dpe record)

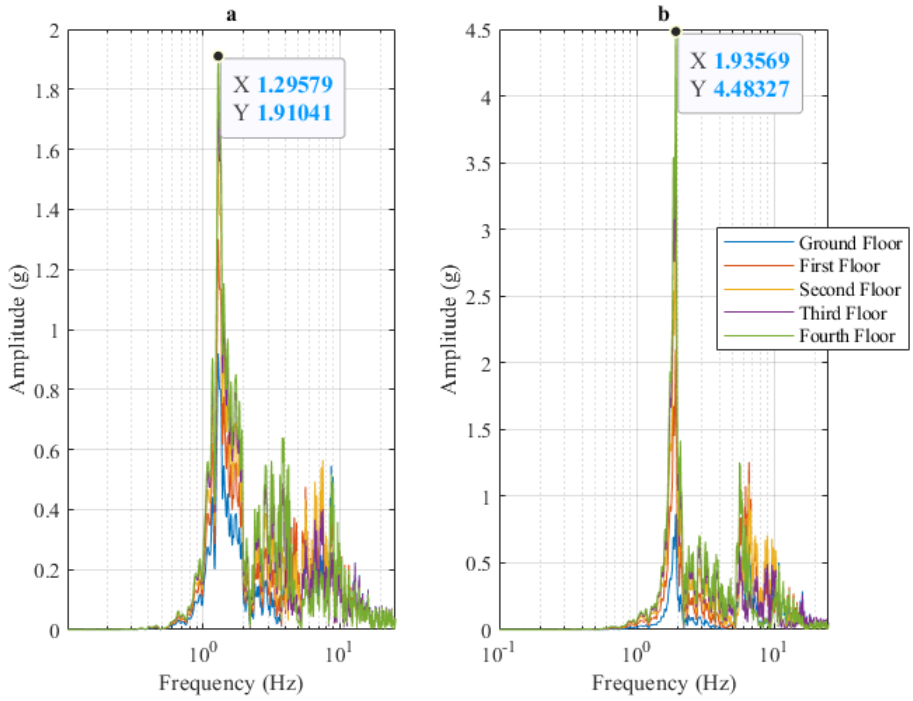


Fig. 14. FFT diagrams of floor accelerations for S1 and S2 models under the Dpe ground motion

Fig. 14 shows the Fourier amplitude spectra for all floors of the S1 and S2 models as the ground moves in the Dpe direction. In the S1 model, the main frequency is around 1.30 Hz, and the peak spectral amplitude is around 1.91 g. The S2 model, on the other hand, has a dominating frequency of about 1.94 Hz, where the spectral amplitude rises to about 4.48 g, which is more than twice the peak amplitude of the S1 model. The dominating frequencies found are close to the fundamental periods found in the modal analysis. For the S1 model, T1 = 0.761 s, and for the S2 model, T1 = 0.518 s. Even though the S2 model has a stronger spectrum amplification at its dominant frequency, the S1 model has higher drift ratios, shear stresses, and tensile–compressive demand levels when the same load is applied.

4. Conclusion

This study investigated the seismic response of two reinforced concrete building models, S1 and S2, designed in compliance with the 1975 Turkish Earthquake Code, employing modal analysis, equivalent seismic load methodologies as outlined in the 1975 and 2018 regulations, linear time-history analyses, and the recorded Defne (Dpe) ground motion. The comparison study focused on the influence of plan layout and stiffness distribution on seismic demand characteristics, rather than on performance-level classification. The results consistently demonstrate that peak acceleration alone is insufficient to characterize a structure's response to an earthquake or the extent of potential damage. The S2 model made acceleration stronger, especially when the load was moving. But this didn't suggest that there was more stress or a change in shape. It was shown that response characteristics based on deformation, like interstory drift distribution and displacement concentration, had an effect on how well the system worked as a whole. The S1 model needs to move more, has more concentrated interstory drifts on the lower levels, and needs additional stress and shear in specific loading scenarios. The key causes for these reaction patterns are that it has a longer fundamental period and a stiffness distribution that isn't as good. Because of this, it is simpler for it to bend in some areas and break when the ground shakes. The S2 model, on the other hand, didn't need as much distortion and had needs that were more equally spaced out. This was because it was stiffer all over and didn't tremble as much when there were earthquakes. Tests in the frequency domain confirmed these results by showing that higher spectrum amplification doesn't always indicate more deformation requirements. This observation underscores the importance of stiffness distribution and deformation patterns in affecting seismic response, rather than merely acceleration amplitude. This study's findings indicate that the configuration and stiffness equilibrium of a structure significantly influence its earthquake resistance when constructed according to outdated seismic regulations. The results show that response characteristics based on deformation are better for comparing seismic assessments than those based on acceleration. They also show us how weak the buildings designed under the Turkish Earthquake Code of 1975 are. This study employed linear elastic analysis; however, the results clearly demonstrate the significant impact of structural configuration and stiffness distribution on seismic demand. To comprehensively assess the reasons for failure and post-yield behavior in reinforced concrete structures constructed in compliance with the 1975 Earthquake Code, nonlinear analysis-based research is recommended as a continuation of this work.

Declaration of conflicting interests

The author(s) declared no potential conflicts of interest with respect to the research, authorship, and/or publication of this article.

Funding

This research received no external funding.

Data availability statement

Data generated during the current study are available from the corresponding author upon reasonable request.

References

[1] Yakut A, Binici B (2023) General properties and seismic performance of high-risk buildings in our country. Çevre, Şehir ve İklim Dergisi 2(4):220–237.

[2] Disaster and Emergency Management Authority (AFAD) (2018) Turkish Building Earthquake Code (TBEC 2018). Ministry of Interior, Republic of Türkiye, Ankara.

[3] Ministry of Public Works and Settlement (2007) Regulation on Buildings to be Constructed in Seismic Zones (DBYBHY 2007). Ankara, Türkiye.

[4] Ministry of Public Works and Settlement (1997) Regulation on Structures to be Constructed in Disaster Areas (ABYYHY 1997). Ankara, Türkiye.

[5] Ministry of Public Works and Settlement (1975) Regulation on Structures to be Constructed in Disaster Areas (ABYYHY 1975). Ankara, Türkiye.

[6] Disaster and Emergency Management Authority (AFAD) (2023) Kahramanmaraş Earthquakes Report (February 6, 2023). Ministry of Interior, Republic of Türkiye.

[7] Gurbuz T, Cengiz A (2025) Structural damages during the February 06, 2023 Kahramanmaraş earthquakes in Turkey. *Soil Dyn Earthq Eng* 191:109214.

[8] Binici B, Yakut A, Kadas K, Demirel O, Akpinar U, Canbolat A, Yurtseven F, Oztaskin O, Aktas S, Canbay E (2023) Performance of RC buildings after Kahramanmaraş earthquakes: lessons toward performance-based design. *Earthq Eng Eng Vib* 22(4):883–894.

[9] Ince O (2024) Structural damage assessment of reinforced concrete buildings in Adıyaman after Kahramanmaraş (Türkiye) earthquakes on 6 February 2023. *Eng Fail Anal* 156:107799.

[10] Buyuksarac A, Isik E, Bektas O (2022) A comparative evaluation of earthquake code change on seismic parameter and structural analysis; a case of Turkey. *Arab J Sci Eng* 47:12301–12321.

[11] Akkar S, Sandıkkaya MA, Bommer JJ (2014) Empirical ground-motion models for point- and extended-source crustal earthquake scenarios in Europe and the Middle East. Bull Earthq Eng 12:359–387.

[12] Wibowo H, Sritharan S (2022) Effects of vertical ground acceleration on the seismic moment demand of bridge superstructure connections. Eng Struct 253:113820.

[13] Katsanos EI, Sextos AG, Manolis GD (2010) Selection of earthquake ground motion records: A state-of-the-art review from a structural engineering perspective. Soil Dyn Earthq Eng 30(2):157–169.

[14] Papazoglou AJ, Elnashai AS (1996) Analytical and field evidence of the damaging effect of vertical earthquake ground motion. Earthq Eng Struct Dyn 30(8):1103–1120.

[15] Gardoni P, Mosalam KM, Der Kiureghian A (2003) Probabilistic seismic demand models and fragility estimates for RC bridges. *J Earthq Eng* 7(S1):79–106.

[16] Lee SH (2019) Evaluation of floor acceleration demands for seismic design of non-structural components. MSc Thesis, Seoul National University, Seoul.

[17] Iervolino I, Manfredi G (2008) A review of ground motion record selection strategies for dynamic structural analysis. In: Modern Testing Techniques of Mechanical and Structural Systems. Springer, Dordrecht.

[18] Dhakal RP, Mander JB, Mashiko N (2006) Identification of critical ground motions for seismic performance assessment of structures. Earthq Eng Struct Dyn 35(8):989–1008.

[19] Pardalopoulos SI, Manolis GD (2021) An engineering approach for evaluating the dynamic response of acceleration-sensitive secondary systems in flexible structures. Earthq Eng Struct Dyn 50(7):1989–2009.

[20] Bayrak E, Celebi O, Kilic M, Ozer C, Aydin AC (2025) The strong ground motion and structural response analysis of 06 February 2023 Pazarcık and Elbistan earthquakes (Mw 7.7 and 7.6): A case study for Malatya-Türkiye, Eastern Anatolia. *Bull Earthq Eng* 23:359–389.

[21] Panzera F, Lombardo G, Imposa S, Catalano S, Romagnoli G, Tortorici G (2018) Correlation between earthquake damage and seismic site effects: The study case of Lentini and Carlentini, Italy. Eng Geol 240:149–162.

[22] Elenas A, Meskouris K (2001) Correlation study between seismic acceleration parameters and damage indices of structures. Eng Struct 23(6):698–704.

[23] Kostinakis K, Athanatopoulou A, Morfidis K (2015) Correlation between ground motion intensity measures and seismic damage of 3D R/C buildings. Eng Struct 82:151–167.
[24] Elenas A (2000) Correlation between seismic acceleration parameters and overall structural damage indices of buildings. Soil Dyn Earthq Eng 20(2):93–100.
[25] Cao VV, Ronagh HR (2014) Correlation between seismic parameters of far-fault motions and damage indices of low-rise reinforced concrete frames. Soil Dyn Earthq Eng 66:102–112.
[26] Poreddy LR, Pathapadu MK, Navyatha C, Vemuri J, Chenna R (2022) Correlation analysis between ground motion parameters and seismic damage of buildings for near-field ground motions. Nat Hazards Res 2:202–209.
[27] Cabañas L, Benito B, Herráiz M (1997) An approach to the measurement of the potential structural damage of earthquake ground motions. Earthq Eng Struct Dyn 26(1):79–92.
[28] Erazo K (2025) Analysis and damage correlation of ground motion intensity measures from records of the 2023 Turkey–Syria earthquake. Bull Earthq Eng 23:1255–1278. https://doi.org/10.1007/s10518-024-01989-8
[29] İnce O (2024) Structural damage assessment of reinforced concrete buildings in Adıyaman after Kahramanmaraş (Türkiye) earthquakes on 6 February 2023. Eng Fail Anal 156:107799.
[30] Altunsu E, Güneş O, Öztürk S, Sorosh S, Sarı A, Toker Beeson S (2024) Investigating the structural damage in Hatay province after Kahramanmaraş-Türkiye earthquake sequences. Eng Fail Anal 157:107857.
[31] Akar F, Işık E, Avcil F, Büyüksaraç A, Arkan E, İzol R (2024) Geotechnical and structural damages caused by the 2023 Kahramanmaraş earthquakes in Gölbaşı (Adıyaman). Appl Sci 14(5):2165. https://doi.org/10.3390/app14052165
[32] Vuran E, Serhatoğlu C, Timurağaoğlu MÖ, Smyrou E, Bal İE, Livaoğlu R (2024) Damage observations of RC buildings from 2023 Kahramanmaraş earthquake sequence and discussion on the seismic code regulations. Bull Earthq Eng 23:1153–1182. https://doi.org/10.1007/s10518-023-01843-3
[33] American Society of Civil Engineers (ASCE) (2017) ASCE/SEI 41-17: Seismic Evaluation and Retrofit of Existing Buildings. Reston, VA.
[34] European Committee for Standardization (CEN) (2004) Eurocode 2: Design of Concrete Structures – Part 1-1: General Rules and Rules for Buildings (EN 1992-1-1). Brussels, Belgium.
[35] Federal Emergency Management Agency (FEMA) (2000) FEMA 356: Prestandard and Commentary for the Seismic Rehabilitation of Buildings. Washington, D.C.
[36] American Society of Civil Engineers (ASCE) (2016) ASCE/SEI 7-16: Minimum Design Loads and Associated Criteria for Buildings and Other Structures. Reston, VA.
[37] Paulay T, Priestley MJN (1992) Seismic Design of Reinforced Concrete and Masonry Buildings. John Wiley & Sons, New York.